J|A|C|S ARTICLES

Published on Web 09/02/2009

Layered Double Hydroxides as Highly Efficient Photocatalysts for Visible Light Oxygen Generation from Water

Cláudia Gomes Silva, Younès Bouizi, Vicente Fornés, and Hermenegildo García*

Instituto de Tecnología Química, UPV-CSIC, Universidad Politécnica de Valencia, Avda. de Los Naranjos s/n, 46022 Valencia, Spain

Received July 8, 2009; E-mail: hgarcia@qim.upv.es

Abstract: Oxygen generation through photocatalytic water splitting under visible light irradiation is a challenging process. In this work we have synthesized a series of Zn/Ti, Zn/Ce, and Zn/Cr layered double hydroxides (LDH) at different Zn/metal atomic ratio (from 4:2 to 4:0.25) and tested them for the visible light photocatalytic oxygen generation. The most active material was found to be (Zn/Cr)LDH with an atomic ratio of 4:2 that exhibits two absorption bands in the visible region at λ_{max} of 410 and 570 nm. It was found that the efficiency of these chromium layered double oxides for oxygen generation increases asymptotically with the Cr content. Using iron oxalate as chemical actinometer we have determined that the apparent quantum yields for oxygen generation (Φapparent = 4 $\times$ mol oxygen/mol incident photons) are of 60.9% and 12.2% at 410 and 570 nm, respectively. These quantum yields are among the highest values ever determined with visible light for solid materials in the absence of light harvesting dye. The overall efficiency of (Zn/Cr)LDH for visible light oxygen generation was found to be 1.6 times higher than that of WO_3 under the same conditions.

Introduction

Visible light photocatalytic water splitting is a topic of much interest because development of efficient hydrogen generation with solar light can be considered a renewable energy resource.[1−4] While there are titanium based photocatalysts that have shown high efficiencies for overall water splitting under UV light illumination, due to the wide band gap, the same materials are notably inefficient under visible light irradiation.[5,6] One general strategy to develop visible light photocatalysts for water splitting that has been widely applied for titanium based semiconductors consists of metal doping in order to introduce energy levels in the band gap. Scheme 1 illustrates the changes in light absorption occurring as consequence of doping and the introduction of energy levels between the conduction and the valence bands of the semiconductor.

Contradictory results on the photocatalytic activity of metal-doped semiconductors have indicated that for similar doping levels different activities can be obtained depending on the experimental protocol used for the preparation of the photocatalyst. It appears that reproducibility is a key point in metal doped semiconductors that makes it difficult to obtain consistent results for similar materials. In addition, doping is an inadequate procedure to introduce a large amount of a metal in a semiconductor material.

Scheme 1. Drawing Illustrating the Effect of Doping on the Absorption Spectra [$F(R)$] and Band Gap Energy (E_g) of TiO_2 Semiconductor

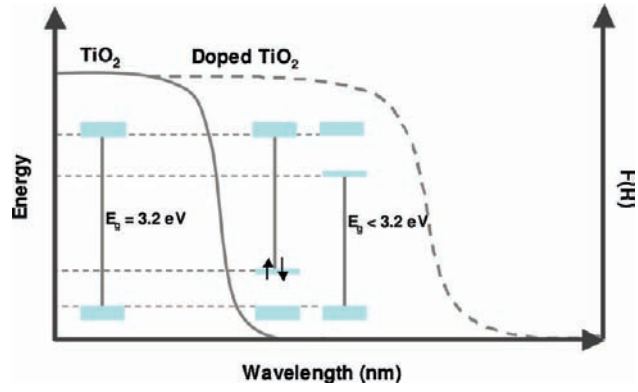

Addressing the issue of a reliable procedure for the preparation of doped semiconductors reaching even larger concentrations of the dopant, in the present manuscript we report the visible light photocatalytic activity of layered double hydroxides (LDHs) commonly known as hydrotalcites. LDHs are brucite-like solids that are constituted by two metals typically having 2+ (M^{II}) and 3+ (M^{III}) or 4+ (M^{IV}) oxidation states, octahedrally surrounded by oxo bridges and hydroxyl groups. The structure is organized forming layers that bear an excess of positive charge equivalent to the number of trivalent or twice the tetravalent metal. This excess of positive charge requires the presence of charge compensating anions that are located in the intergallery spaces. Figure 1 shows a schematic illustration of the general LDH structure.

An advantage of the hydrotalcites is that they can be prepared in large quantities in a reliable and reproducible manner by

(1) Matsuoka, M.; Kitano, M.; Takeuchi, M.; Tsujimaru, K.; Anpo, M.; Thomas, J. M. *Catal. Today* **2007**, *122*, 51–61.
(2) Ni, M.; Leung, M. K. H.; Leung, D. Y. C.; Sumathy, K. *Renewable Sustainable Energ. Rev.* **2007**, *11*, 401–425.
(3) Nowotny, J.; Sorrell, C. C.; Sheppard, L. R.; Bak, T. *Int. J. Hydrogen Energy* **2005**, *30*, 521–544.
(4) Tributsch, H. *Int. J. Hydrogen Energy* **2008**, *33*, 5911–5930.
(5) Kudo, A. *Int. J. Hydrogen Energy* **2007**, *32*, 2673–2678.
(6) Kudo, A.; Miseki, Y. *Chem. Soc. Rev.* **2009**, *38*, 253–278.

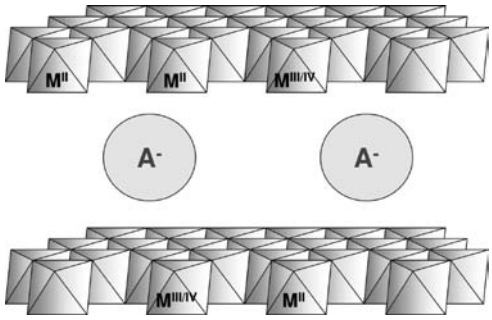

Figure 1. LDH structure with stacking of brucite-like layers. M^{II} and $M^{III/IV}$ represent the divalent and tri/tetravalent element and A^- the anion in the intergallery space compensating for the charge introduced by $M^{III/IV}$.

precipitation of aqueous solutions of the corresponding metal salts by increasing the solution pH. In addition, the atomic ratio between the divalent and tri- or tetravalent metal ions of the double oxide can be varied in a wide range without altering the structure of the material.[7]

LDHs, particularly those having carbonate as compensating anions or transition metals in the layers, have been widely used as heterogeneous catalysts for base-catalyzed reactions or redox transformations.[8−14] However, the photocatalytic properties of these materials have been mostly ignored.[15−17] With the consideration that LDHs have two different metals and that the proportion between these two metals can be controlled, LDHs can be envisioned as providing the opportunity of having "doped semiconductors". For instance, when the higher valent metal is titanium or when the divalent metal is zinc, materials analogous to titania and zinc oxide can be obtained but with the advantage that the "dopant" metal would be present in well-defined structural positions. In this way, the location of the dopant on the semiconductor oxide can be precisely determined while the solid is easily reproducible.

In the present work, we have developed this novel concept of doped semiconductor based on LDHs by preparing a series of hydrotalcite zinc oxides and studying their activity for visible light photocatalytic oxygen generation. The overall water splitting is constituted by two independent semireactions, one of which being the formation of H_2 is significantly more feasible and occurring generally with high efficiencies compared to the O_2 evolution.[18,19] For this reason and in order to test the use of LDHs as visible light photocatalysts, we have selected O_2 evolution as a challenging process to determine the relative efficiency of our materials.

Scheme 2. Preparation Procedure Followed To Obtain the Materials Used as Visible Light Photocatalysts for O_2 Production

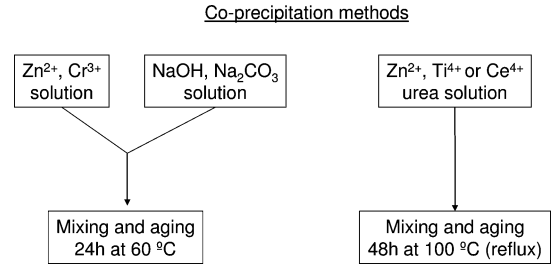

Experimental Section

LDH Preparation. Two methods were used for material preparation. The first one is the coprecipitation of metal salts from aqueous solution with NaOH solution for the incorporation trivalent element (Cr^{3+}, Al^{3+}). The second procedure has been used for the incorporation of tetravalent elements (Ti^{4+}, Ce^{4+}) and consists of the continuous release of ammonia by urea decomposition in water at moderate temperatures. All the reactants used for the preparation of the LDH materials are analytical grade chemicals. Scheme 2 summarizes the preparation procedure followed to obtain three types of LDHs used in this work.

Zn−Cr LDH. The synthesis procedure is based on the coprecipitation method with NaOH solution. It has been reported that LDH materials with high crystallinity are obtained when M^{II}/M^{III} atomic ratio is 2. If higher M^{II}/M^{III} ratios are used, phase segregation and loss of crystallinity may occur. In order to avoid this problem and obtain highly crystalline LDHs while varying the Zn^{2+}/Cr^{3+} ratio we have prepared different samples containing also Al^{3+} in which the $Zn^{2+}/(Al^{3+} + Cr^{3+})$ was constantly 2:1 and relative Al^{3+} versus Cr^{3+} was varied. A solution of $Zn(NO_3)_2 \cdot 6H_2O$ and $Cr(NO_3)_3 \cdot 6H_2O$ with Zn/Cr ratio of 2 in deionized water (60 mL, $[Zn^{2+} + Cr^{3+}] = 2$ M) was added drop by drop in NaOH and Na_2CO_3 solution (80 mL, [NaOH] = 3 M and $[Na_2CO_3] = 2.5$ M). The mixture was aged 24 h at 60 °C. The solid was recovered by filtration and washed copiously with distilled water. The sample was dried at 60 °C and then stored at room temperature. Some samples have been calcined at 450 °C under an air atmosphere (2 h). Knowing that the optimum Zn/M^{III} ratio should be 2:1, we prepared other materials by substituting a part of Cr^{3+} by Al^{3+}. In this way, three other (Zn/Cr/Al)LDH materials were prepared in which the Zn/Cr atomic ratio was 4:1.75, 4:1, and 4:0.25 and the Zn/Al ratio was 4:0.25, 4:1, and 4:1.75. These three (Zn/Cr/Al)LDH materials were obtained using the same procedure as (Zn/Cr)LDH but using $Al(NO_3)_3$ as aluminum source and keeping the $[Zn^{2+} + Cr^{3+} + Al^{3+}] = 2$ M.

Zn−Ti and Zn−Ce LDHs. The synthesis protocol is based on the method used in previous publications.[20,21] The materials were prepared by coprecipitation of the $Zn(NO_3)_2 \cdot 6H_2O$ metal salt with cerium or titanium isopropoxide ($M^{II}/M^{IV} = 6:1$, $[M^{II} + M^{IV}] = 0.7$ M) in a solution of urea (1 M) heated at 100 °C for 48 h under reflux. The hydrolysis of urea forms ammonium cyanate, which is later hydrolyzed into ammonium carbonate. The hydrolysis of ammonium and carbonate ions gives, respectively, ammonia and hydrogen carbonate and results in a pH of about 9. The hydrolysis of urea proceeds very slowly which allows for preparing material with a better crystallinity and a better control of the particle size. This method is not suitable for the (Zn/Cr)LDH preparation.[22] The

(7) Evans, D. G.; Slade, R. C. T. In *Structure and Bonding (Berlin)*; Mingos, D. M. P., Ed.; Springer: New York, 2005; Vol. 119, pp 4−11.
(8) Cavani, F.; Trifirò, F.; Vaccari, A. *Catal. Today* **1991**, *11*, 173–301.
(9) Martin, K. J.; Pinnavaia, T. J. *J. Am. Chem. Soc.* **1986**, *108*, 541–542.
(10) Pinnavaia, T. J. *Science* **1983**, *220*, 365–371.
(11) Reichle, W. T. *J. Catal.* **1985**, *94*, 547–557.
(12) Reichle, W. T.; Kang, S. Y.; Everhardt, D. S. *J. Catal.* **1986**, *101*, 352–359.
(13) Vaccari, A. *Catal. Today* **1998**, *41*, 53–71.
(14) Centi, G.; Perathoner, S. *Microporous Mesoporous Mater.* **2008**, *107*, 3–15.
(15) Guo, Y. H.; Li, D. F.; Hu, C. W.; Wang, E.; Zou, Y. C.; Ding, H.; Feng, S. H. *Microporous Mesoporous Mater.* **2002**, *56*, 153–162.
(16) Kun, R.; Balazs, M.; Dekany, I. *Colloids Surf., A* **2005**, *265*, 155–162.
(17) Meng, W. Q.; Li, F.; Evans, D. G.; Duan, X. *J. Porous Mater.* **2004**, *11*, 97–105.
(18) Kanan, M. W.; Surendranath, Y.; Nocera, D. G. *Chem. Soc. Rev.* **2009**, *38*, 109–114.
(19) Kanan, M. W.; Nocera, D. G. *Science* **2008**, *321*, 1072–1075.
(20) Saber, O.; Tagaya, H. *J. Inclusion Phenom. Macrocyclic Chem.* **2003**, *45*, 109–116.
(21) Saber, O.; Tagaya, H. *J. Porous Mater.* **2009**, *16*, 81–89.
(22) Costantino, U.; Marmottini, F.; Nocchetti, M.; Vivani, R. *Eur. J. Inorg. Chem.* **1998**, 1439–1446.

solids were recovered by filtration, washed with distilled water, and dried at 60 °C overnight.

Materials Characterization. Powder X-ray diffraction (XRD) was recorded on a Philips Cubix Pro using Cu Kα radiation at 45 kV and 40 mA in the 2θ range from 5° to 70°. Room temperature diffuse reflectance UV−vis−NIR spectra of solid samples were recorded with a Varian Cary 5000 UV−vis−NIR scanning spectrophotometer. The chemical composition of the LDHs was determined with an inductively coupled plasma-optical emission spectrometer (ICP-OES, Varian). SEM images were obtained using a JEOL JSM-6300 microscope operating at 20 kV. EDX analysis was performed in an Oxford Instruments INCA analyzer.

Photocatalytic Tests. The photocatalytic experiments were carried out in a 30 mL pyrex reactor filled with 22.5 mL of aqueous suspension. The headspace of the reactor was connected to an inverted buret filled with water at atmospheric pressure, allowing the measurement of the evolved O_2 volume. LDH powders (45 mg) were dispersed in a 0.01 M $AgNO_3$ solution in the reaction cell. The suspensions were purged with an argon flow for at least 30 min before irradiation in order to remove dissolved air. Then the suspensions were irradiated for 3 h using a 200 W xenon-doped mercury lamp (Hamamatsu Lightningcure LC8). A cutoff filter was employed for visible light irradiation ($\lambda > 400$ nm). The stationary temperature of the reactor was 38 °C. The formation of oxygen was confirmed by injecting 0.5 mL of the reactor headspace gas in a gas chromatograph (HP 5890) operating at isothermal conditions (50 °C) using a semicapillary column (molecular sieve, 530 μm diameter, 15 m length) equipped with a thermal conductivity detector. Photon flux was determined at 410 and 570 nm using a monochromator (half width 12 nm) by potassium ferrioxalate actinometry.[23]

Results and Discussion

A simple rationalization to consider the photocatalytic activity of LDH solids is to view the material as zinc oxide semiconductor doped with the tri- or tetravalent metal ion that introduces some extra levels in the energy band gap of the semiconductor. In addition the layered structure allows water sorption and swelling, increasing significantly the surface area available for the photocatalysis.

The layered materials were characterized by powder XRD, where the expected $d(003)$ peak characteristic of the diffraction pattern of layered solids was recorded. Figure 2 shows the powder XRD of the LDHs used in the present study. In the case of (Zn/Cr)LDH, XRD showed also the reflection of the planes (006), (101), and (110) at 2θ 24°, 34°, and 39° which are typically encountered in LDH materials (see Figure 2a).[24] These peaks disappear after calcination of (Zn/Cr)LDH at 450 °C, and new peaks at higher 2θ values were observed (Figure 2d). On the basis of the XRD of calcined (Zn/Cr)LDH the formation of zinc oxide and a spinel ($ZnCr_2O_4$) phase was determined. Figure 2b shows that the (Zn/Ti)LDH has a lamellar structure equivalent to the phase described in previous publication[20] in which Ti^{4+} was incorporated in the layered structure of the material. The XRD pattern of the (Zn/Ce)LDH indicates that, besides (Zn/Ce)LDH, a second phase consisting of cerium oxide carbonate hydrate is present. This indicates that a part of Ce^{4+} cation is not in the lamellar structure. Nevertheless, this material is still interesting as a photocatalyst due to the good dispersion of both phases $Ce_2O(CO_3)_2 \cdot H_2O$ and (Zn/Ce)LDH.

The materials were further characterized by elemental analysis that established the composition and the atomic ratio between the metals. Table 1 summarizes the elemental and structural information of the three materials.

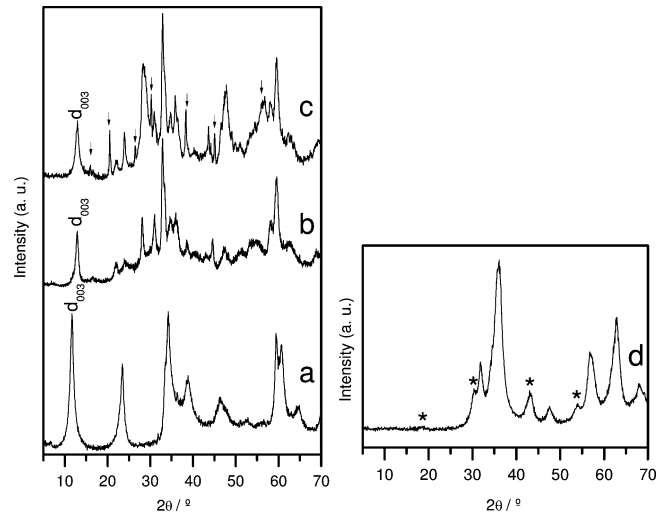

Figure 2. Powder X-ray diffraction pattern of (a) (Zn/Cr)LDH, (b) (Zn/Ti)LDH, (c) (Zn/Ce)LDH (↓ indicates the peaks corresponding to cerium oxide carbonate hydrate), and (d) (Zn/Cr)LDH calcined at 450 °C that corresponds to a mixture of two solid phases (ZnO + * $ZnCr_2O_4$).

Table 1. Chemical Composition of the Materials Used as Visible-Light Photocatalysts for O_2 Production

sample	Zn (wt%)	Cr (wt%)	Ti (wt%)	Ce (wt%)	$Zn/M^{III/IV}$	structure
(Zn/Cr)LDH	47.4	18.8			2:1	layered structure
(Zn/Ti)LDH	63.2		6.1		7.6:1	Ti^{4+} in the layered structure
(Zn/Ce)LDH	54.1			13.3	8.7:1	presence of $Ce_2O(CO_3)_2 \cdot H_2O$

Because of our interest in testing the photocatalytic activity, the optical spectrum provides important information. Figure 3 shows the diffuse reflectance UV−vis spectra of the three types of LDHs used in this study. As can be seen there, (Zn/Ce)LDH shows a peak at about 280 nm with a tail expanding into the visible region. (Zn/Ti)LDH has the most intense band occurring at 304 nm. In sharp contrast, (Zn/Cr)LDH exhibits two maxima in the visible region at 410 and 570 nm, respectively. According to this data and considering that our target is to determine the photocatalytic activity under visible light ($\lambda > 400$ nm), it appears that (Zn/Cr)LDH is the most promising material for

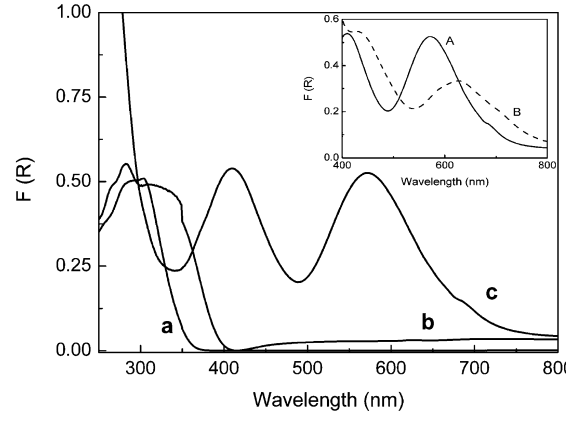

Figure 3. Diffuse reflectance UV−vis spectra (plotted as the Kubelka−Munk function of the reflectance, R) of (a) (Zn/Ti)LDH, (b) (Zn/Ce)LDH, and (c) (Zn/Cr)LDH. Inset: Diffuse reflectance UV−vis spectra of (Zn/Cr)LDH (A) before and (B) after calcination at 450 °C.

(23) Braun, A. M.; Maurette, M.-T.; Oliveros, E. *Photochemical Technology*; John Wiley & Sons: Chichester, U.K., 1991.
(24) Roussel, H.; Briois, V.; Elkaim, E.; de Roy, A.; Besse, J. P.; Jolivet, J. P. *Chem. Mater.* **2001**, *13*, 329–337.

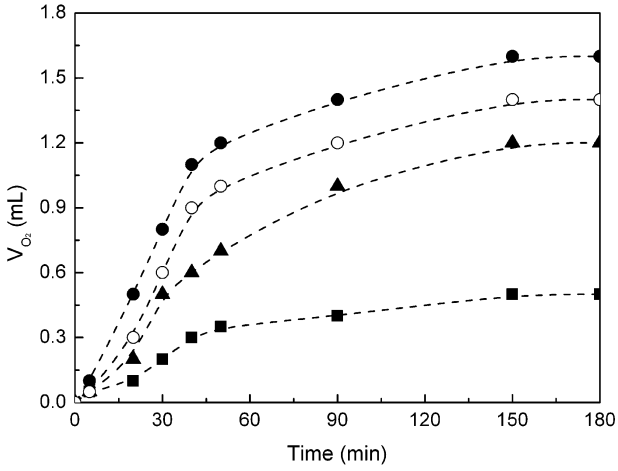

Figure 4. Temporal profile of the volume of oxygen evolved during the irradiation of aqueous suspensions of (Zn/Cr)LDH (●), calcined (Zn/Cr)LDH (○), (Zn/Ce)LDH (▲), and (Zn/Ti)LDH (■) using 10^{-2} M $AgNO_3$ as sacrificial acceptor.

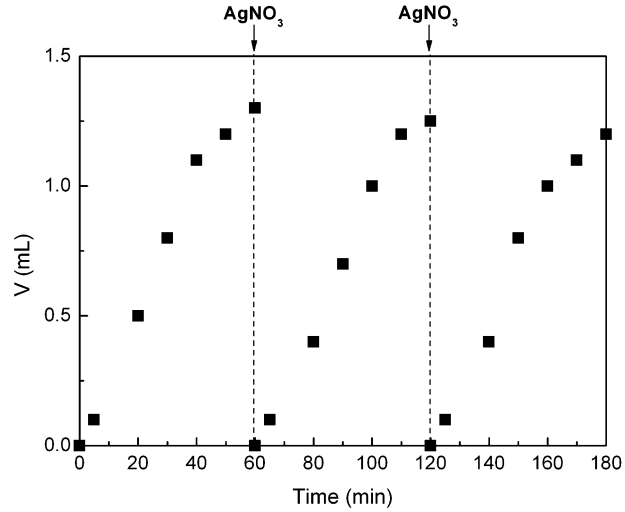

Figure 5. Volume of O_2 formed vs irradiation time in three consecutive cycles in which additional amounts of $AgNO_3$ have been added every 60 min (reaction conditions: total suspension volume = 22.5 mL; (Zn/Cr)LDH photocatalyst; m_{cat} = 45.0 mg; [$AgNO_3$] = 0.01 M).

this purpose because it presents two intense absorptions in the visible region.

For the sake of comparison and in order to address the influence of structure on the photocatalytic activity, we submitted (Zn/Cr)LDH to calcination at 450 °C. It is well-known that LDHs are thermally labile, and upon calcination at temperature above 400 °C, they undergo phase transformation into $ZnCr_2O_4$ spinels and independent metal oxide phase of the divalent cation. Figure 2d shows also the XRD of the material resultant after the thermal treatment of (Zn/Cr)LDH in where the disappearance of layered structure and the presence of ZnO together with $ZnCr_2O_4$ spinels is clearly shown, while the inset of Figure 3 shows the optical spectrum of the resulting solid upon calcination of (Zn/Cr)LDH.. As can be seen in the inset of Figure 3, the two absorption bands in the visible characteristic of (Zn/Cr)LDH shifts to the red and broadens upon calcination.

Comparison of the photocatalytic activity of fresh and calcined (Zn/Cr)LDH will serve to discuss the influence on photocatalytic activity of well-defined structure as in the case of LDH with respect to that of a $ZnCr_2O_4$ spinel mixed oxide phase impurified with zinc oxide.

Initially we addressed the influence of the M^{III} ion (Ti, Ce, or Cr) on the photocatalytic activity of the (Zn/M)LDH. For this purpose we determined the visible light photocatalytic oxygen generation of (Zn/Cr)LDH, (Zn/Ce)LDH, and (Zn/Ti)LDH under the same conditions. The results are given in Figure 4. As can be seen there, the zinc LDH containing chromium was found to be the most active material. These results can be easily interpreted on the basis of the optical spectra of the three types of LDHs. As commented earlier, there are remarkable variations in the light absorption of the zinc LDHs depending on the nature of the $M^{III/IV}$. Actually, (Zn/Cr)LDH is the material with the most intense absorption in the visible region, where irradiation is carried out. In contrast, (Zn/Ti)LDH is the material with lesser visible absorption and accordingly is the solid showing the lowest photocatalytic activity for O_2 generation with white visible light.

In a comparison of the photocatalytic activity of (Zn/Cr)LDH and the material resulting from its calcination at 450 °C, it is observed that the calcined material, in which well-defined structure typical of LDH materials is lost, has diminished its photocatalytic activity with respect to (Zn/Cr)LDH. Figure 4 shows the corresponding plots of the temporal O_2 evolution under the same conditions. This comparison nicely illustrates the advantages of using as photocatalyst a LDH material having its structural integrity intact. The importance of the layered hydrotalcite structure must derive from its ability to sorb water and effect swelling in various degrees. Thus, water should be able to access to the intergallery space as well as the external nongallery surface. This maximizes the surface of the material accessible for the photocatalytic oxygen generation. Nevertheless it is noticeable that the activity of the calcined material is still remarkable, probably due to the activity of Cr,Zn spinel generated in the calcination process. Moreover, the activity of the calcined (Zn/Cr)LDH is still higher than that of the other two (Zn/M)LDH (M = Ce and Ti) materials. This higher activity of calcined (Zn/Cr)LDH with respect to (Zn/Ce)LDH and (Zn/Ti)LDH can be rationalized considering that illumination is carried out with visible light and that, due to their chemical composition and in contrast to calcined (Zn/Cr)LDH, the two hydrotalcites containing Ce and Ti do not exhibit much light absorption in the visible region.

As it can be seen in Figure 4, which represents the temporal evolution of O_2 formation, the volume of oxygen evolved in the photocatalytic reaction tends asymptotically to a maximum value at long irradiation times. We interpreted this profile as due to the depletion of Ag^+ that is the sacrificial electron acceptor agent in the process. In this context it is worth commenting that control experiments of the photocatalytic oxygen generation of (Zn/Cr)LDH in the absence of Ag^+ only forms very small amounts of oxygen (<0.1 mL in 180 min).

To demonstrate that the photocatalyst is still active without decay in its activity at long irradiation times and that the photocatalytic process tends to stop due to the lack of electron acceptor, we proceeded to add periodically additional amounts of $AgNO_3$ and determine the O_2 evolution in these consecutive cycles. Figure 5 shows the oxygen volume evolved in the reaction as a function of time when additional amounts of $AgNO_3$ are added. As can be seen there, once the photocatalytic reaction tends to stop, addition of $AgNO_3$ reactivates again the evolution of O_2, indicating that it is $AgNO_3$ depletion and not the deactivation or corrosion of the catalyst that is the reason for the cease in O_2 evolution. However, we noticed that the

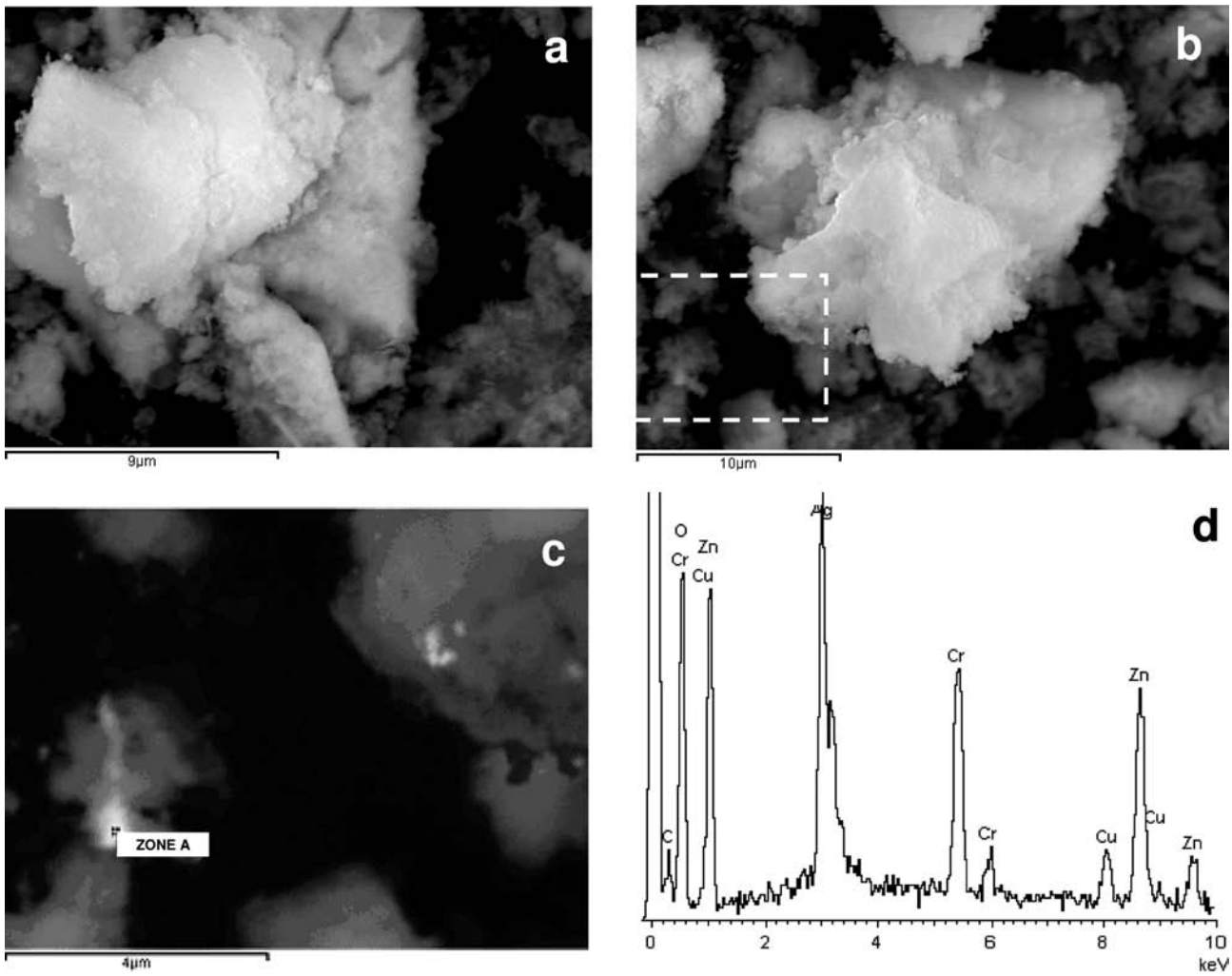

Figure 6. SEM images of (a) (Zn/Cr)LDH photocatalyst before its use, (b) (Zn/Cr)LDH employed as photocatalyst for O_2 generation using $AgNO_3$ as sacrificial electron acceptor, (c) magnification of the dashed area showed in part b in which the presence of silver deposits appear as light spots (backscattered electron image), (d) EDX analysis of the point indicated in image c and where the presence of Ag is detected.

initial rate becomes gradually slower, suggesting that the Ag nanoparticles originated as side product from the reduction of Ag^+ cause some deactivation of the photocatalyst. It was, however, determined that Ag^+ as electron acceptor is more advantageous than persulfate. Using persulfate as sacrificial electron acceptor agent, the oxygen evolution was identical to that measured for Ag^+ during the first 30 min of operation (see Supporting Information Figure S1). However, upon prolonged exposure, the photocatalytic activity using persulfate declined faster than with Ag^+ and visually it was observed that the (Zn/Cr)LDH becomes damaged. It is probable that the high oxidation potential of persulfate causes some corrosion of the material.

In order to provide some experimental evidence in support of the deposition of Ag nanoparticles on the (Zn/Cr)LDH during the photocatalytic water splitting, we performed SEM coupled with EDX analysis of the (Zn/Cr)LDH photocatalyst after the reaction. Figure 6 compares the SEM images before and after the reaction as well as the result of the elemental analysis obtained by EDX. As can be seen in this figure, while the morphology of the (Zn/Cr)LDH particles is not changed during the photocatalytic reaction, the presence of significant amounts of Ag metal particles can be observed in the used material, thus confirming the deposition of Ag on the surface of the used (Zn/Cr)LDH. We propose that the presence of these Ag nanoparticles deposited on the (Zn/Cr)LDH surface is the origin of the slow deactivation observed for (Zn/Cr)LDH.

To optimize oxygen generation using (Zn/Cr)LDH we determined the O_2 volume as a function of time for a series of experiments varying the amount of photocatalyst. In heterogeneous photocatalysis using suspensions of opaque solids it is commonly observed that, upon increasing the amount of solid in the suspension, an increase in the photocatalytic activity is observed until a maximum in efficiency is achieved.[25] Beyond this concentration of solid photocatalyst for maximum efficiency, a decrease in the photocatalytic activity is typically observed. This volcano curve correlating photocatalytic efficiency and photocatalyst loading is typically interpreted as arising from the balanced combination of two opposite phenomena. On one hand light absorption by the solid increases with the concentration of solid until most of the photons entering in the system are absorbed. The beneficial influence of photocatalyst concentration on light absorption is responsible for the increase in the photocatalytic efficiency with photocatalyst loading. However, a certain concentration is reached for which additional loadings of photocatalyst do not increase light absorption. On the contrary additional amounts of the opaque photocatalyst reduce transpar-

(25) Herrmann, J. M. *Top. Catal.* **2003**, *34*, 49–65.

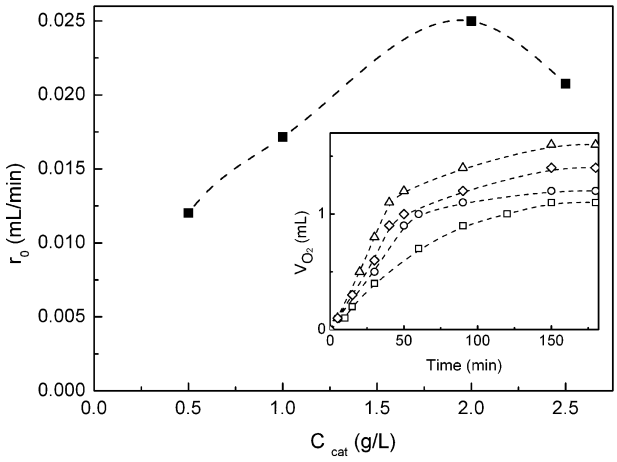

Figure 7. Initial rate of oxygen production (r_0) obtained for different (Zn/Cr)LDH loadings. The inset shows the volume of O_2 evolved during the photocatalytic irradiation of suspensions containing different concentrations of (Zn/Cr)LDH: □ 0.5 g/L, ○ 1.0 g/L, Δ 2.0 g/L, ◇ 2.5 g/L .

ency and produce light scattering, light reflection, and other physical phenomena that influence negatively the photocatalytic efficiency. This optimal photocatalyst loading depends on the photocatalytic reactor and the geometry of the system and has to be determined in each case.

Aimed at determining the optimal (Zn/Cr)LDH loading in our system for the maximum O_2 generation, we performed a series of photocatalytic experiments in where the concentration of (Zn/Cr)LDH was varied from 0.5 to 2.5 g/L. Optimal (Zn/Cr)LDH loading was determined by plotting the initial rate of oxygen generation measured from the slope at zero time of the O_2 volume versus time curve. Figure 7 presents the influence of the photocatalyst loading on the initial rate of oxygen generation where a concentration of 2 g/L was found to give the highest photocatalytic activity for our system under the conditions used.

After having determined the best photocatalyst loading for O_2 generation, we proceeded to perform a study under these conditions to assess the influence of Cr content on the photocatalytic activity of (Zn/Cr)LDH. As mentioned in the introduction, one of the major advantages of using LDHs as materials is the possibility to vary during the synthesis the Zn/Cr ratio by incorporating a new M^{III} metal atom substituting Cr^{3+}. Considering that Cr plays an important role in the photocatalytic activity, it was of interest to disclose which is the optimum Cr content in the material within the available range allowed by the LDH synthetic procedure (maximum Zn/Cr ratio of 2:1). When Cr content is varied, a photocatalyticaly inactive M^{III} atom such as Al^{3+} was introduced in the material in order to maintain constant M^{II}/M^{III} ratio while changing the Cr content. Aluminum is considered an inert metal since alumina and other aluminum oxides are devoid of any photocatalytic activity. Four (Zn/Cr)LDHs with Zn/Cr ratio varying from 4:0.25 to 4:2 were prepared. The photocatalytic activity is presented in Table 2 in which the photoactivity of (Zn/Ti)LDH and (Zn/Ce)LDH has also been included for comparison.

As can be seen in Table 2, the photocatalytic activity of (Zn/Cr)LDH increases gradually along the Cr content of the solid, the best performing LDH being the one with the maximum possible Cr loading. However, we notice that there is not a linear relationship between the concentration of Cr in the solid and the initial reaction rate or the total amount of O_2 evolved at 3 h. Thus, it can be assumed that a plateau would be reached in

Table 2. Oxygen Production at 3 h of Irradiation and Initial Oxygen Production Rate (r_{0,O_2})[a]

material	x[b]	$O_{2,3\ h}$ (μmol)	r_{0,O_2} (μmol/h/g)
(Zn/Ce)LDH		48.3	626.1
(Zn/Ti)LDH		20.1	268.3
(Zn/Cr)LDH	4:2	64.4	1073.3
(Zn/Cr)LDH	4:1.75	56.3	894.4
(Zn/Cr)LDH	4:1	52.3	805.0
(Zn/Cr)LDH	4:0.25	44.2	715.5

[a] Obtained with the different LDH materials (reaction conditions: total suspension volume = 22.5 mL; m_{cat} = 45.0 mg; [$AgNO_3$] = 0.01 M). [b] M^{II}:M^{III}

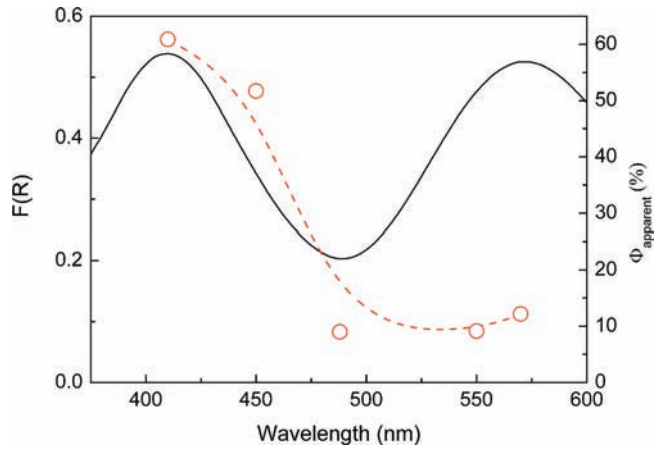

Figure 8. Diffuse reflectance UV−vis spectra (plotted as the Kubelka−Munk function of the reflectance, R, left vertical axis) of (Zn/Cr)LDH and apparent quantum yield ($\Phi_{apparent}$) of incident photon to oxygen conversion (○, right vertical axis).

which an additional increase in the Cr content would lead only to a negligible improvement in the photocatalytic efficiency for oxygen generation. In this context, it is worth commenting that, from the material point of view, also the Zn to Cr atomic ratio can be varied in a certain range and the maximum concentration of Cr in the LDH structure is the one corresponding to a Zn/Cr atomic ratio of 2:1.

As mentioned earlier when discussing the optical spectra of chromium LHDs and the origin of the visible light photocatalytic activity, (Zn/Cr)LDH exhibits two absorption bands in the visible region at λ_{max} 410 and 570 nm, respectively. In the context of the photocatalytic efficiency of the (Zn/Cr)LDH materials, we were interested in determining the apparent quantum yield for O_2 generation using monochromatic light of wavelengths corresponding to the maxima of the absorption bands. Quantum yield of incident photon to oxygen conversion is the most appropriate parameter to establish the photocatalytic efficiency. Data of the volume of oxygen evolved for a certain period of time under certain conditions makes comparison of the photocatalytic activity of solids prepared by different authors very problematic and subject to erroneous conclusions. Using potassium ferrioxalate as chemical actinometer we have determined the quantum yield for O_2 generation. Figure 8 presents the obtained values of incident photon to oxygen conversion efficiency for several wavelengths. The high quantum yields, particularly at 410 nm (60.9%), for O_2 generation are quite remarkable and places (Zn/Cr)LDH at the top of the list of the most efficient photocatalysts for visible light water splitting.[26−28]

(26) Hitoki, G.; Takata, T.; Kondo, J. N.; Hara, M.; Kobayashi, H.; Domen, K. *Chem. Commun.* **2002**, 1698–1699.

The different quantum yields obtained for the two visible absorption bands of (Zn/Cr)LDH can be due to the different nature of the electronic transition promoted at each wavelength.

In this regard, with the precedents in the literature under consideration, both the 410 and 570 nm bands have been attributed to ligand to metal transitions in octahedral Cr ions.[29] Apparently, the 410 nm band corresponding to a charge transfer band from oxygen atoms of the lattice to the metal ions leads to a more efficient charge separation with the creation of electrons and holes in the semiconductor.

Using the same chemical actinometer we also determined the quantum yield for O_2 generation of (Zn/Ti)LDH and (Zn/Ce)LDH at 410 nm whereby 15.1% and 37.8% were obtained, respectively. Although these quantum yields are also quite remarkable, they are significantly lower than the one determined for (Zn/Cr)/LDH.

Besides quantum efficiency determination, we wanted to provide a comparison of the relative efficiency of (Zn/Cr)LDH for the visible light photocatalytic oxygen generation with a reference material under exactly the same conditions. For this comparison we selected WO_3 that is a widely used photocatalyst for oxygen generation. Ohtani and co-workers have reported the formation of 12 μmol of O_2 under 2 h of visible-light irradiation ($\lambda > 420$ nm) using a 400 W high-pressure mercury source, a WO_3 loading of 10 g/L, and Ag_2SO_4 (0.005 M) as sacrificial agent.[30] For comparison purposes, and following the procedure described in that work, we prepared a sample of WO_3 by hydrothermal treatment of an aqueous tungstic acid solution (H_2WO_4 99%, Aldrich) during 1 h at 823 K (10 K/min rate). The diffuse reflectance UV−vis spectrum of the WO_3 material is shown in Supporting Information (Supporting Information Figure S2). XRD analysis confirmed that the material consists of monoclinic WO_3.

Comparison of the photocatalytic activity for oxygen generation of (Zn/Cr)LDH and WO_3 was performed under the conditions employed here throughout the work, i.e., 2 g/L of photocatalyst loading and 0.01 M of $AgNO_3$ using a 200 W xenon-doped Hg lamp with a cutoff filter for $\lambda > 400$ nm. It was determined that the WO_3 standard exhibits 0.61 times lower efficiency for photocatalytic oxygen generation than (Zn/Cr)LDH, as determined from the slope of the temporal oxygen evolution (see Supporting Information Figure S3). This higher efficiency of (Zn/Cr)LDH can be attributed to the structural features allowing water sorption inside the particle and light absorption properties of the layered double hydroxide material in the visible spectral range.

Conclusion

Hydrotalcites are very well described mixed oxides that can be easily prepared in large scale in a reliable and reproducible manner. The use of these layered double hydroxides as photocatalysts has been mostly neglected up to now. However, the present results show that these solids have vast potential as visible light photocatalysts. All the materials prepared exhibit quite remarkable photocatalytic activity, with the one containing Zn and Cr as the most active. We have found that the concentration of Cr plays a beneficial role in photocatalytic activity. By using monochromatic light, an apparent quantum yield for O_2 generation as high as 60.9% has been measured at 410 nm. This value is probably one of the highest ever reported for the photocatalytic O_2 generation in the visible region.

Acknowledgment. Financial support by the Spanish Ministry of Science and Innovation (CTQ2009-11583) is gratefully acknowledged. Cláudia G. Silva thanks Fundação para a Ciência e a Tecnologia (Portugal) for the postdoctoral fellowship (SFRH/BPD/48777/2008).

Supporting Information Available: Three figures showing the relative efficiency of (Zn/Cr)LDH using Ag^+ or $S_2O_8^{2-}$ as sacrificial electron acceptor, the optical spectrum of monoclinic WO_3 solid, and relative efficiency of (Zn/Cr)LDH and WO_3 under the same experimental conditions. This material is available free of charge via the Internet at http://pubs.acs.org.

JA905467V

(27) Kim, H. G.; Hwang, D. W.; Lee, J. S. *J. Am. Chem. Soc.* **2004**, *126*, 8912–8913.
(28) Kudo, A.; Ueda, K.; Kato, H.; Mikami, I. *Catal. Lett.* **1998**, *53*, 229–230.
(29) del Arco, M.; Rives, V.; Trujillano, R.; Malet, P. *J. Mater. Chem.* **1996**, *6*, 1419–1428.
(30) Kominami, H.; Yabutani, K.; Yamamoto, T.; Kara, Y.; Ohtani, B. *J. Mater. Chem.* **2001**, *11*, 3222–3227.